

Direct transition to elastoinertial turbulence from a linear instability in channel flow

Lu Zhu and Li Xi*

Department of Chemical Engineering, McMaster University, Hamilton, Ontario L8S 4L7, Canada

(Dated: November 18, 2022)

For decades, transition to turbulence in viscoelastic parallel shear flows was believed to require nonlinear instabilities. We provide numerical evidences for a new wall-mode linear instability that directly triggers the transition to elastoinertial turbulence in channel flow. The instability is 2D but 3D features become important as nonlinear effects grow. With larger disturbances, direct transition to nonlinear instabilities, leading to turbulent states of both inertial and elastoinertial natures, are observed.

In Newtonian fluids, turbulence kicks in when fluid inertia overpowers viscous dissipation to trigger flow instabilities. The transition is nonlinear in pipe flow, for which a finite-amplitude disturbance is required. In channel flow, although the laminar state becomes linearly unstable at the Reynolds number $Re = 5772$, where bifurcation to the Tollmien-Schlichting (TS) wave occurs [1], transition to turbulence occurs at a much lower $Re_c \approx 1000$ [2], highlighting the essential role of nonlinear instabilities.

Dilute polymer solutions are viscoelastic. Their turbulence can show much lower friction drag, which is known as the drag reduction (DR) phenomenon [3, 4]. In those flows, according to the most common explanation, turbulence is still driven by inertia (inertia-driven turbulence – IDT) but its fluctuations are suppressed by polymer stress [5–8]. A different mechanism emerged recently with the discovery of the so-called elastoinertial turbulence (EIT) where both inertia and elasticity support turbulent instabilities [9]. EIT dominates at the high-elasticity limit and is critical for answering the most important questions in the field, including the maximum drag reduction (MDR) phenomenon [10, 11]. Transition to EIT can occur at lower Re_c (early transition) than the laminar-turbulent transition in Newtonian flow [10, 12]. This reignited the question of whether turbulent transition can be triggered by a linear instability in viscoelastic parallel shear flow.

The answer so far has been no. Although viscoelastic fluids can show turbulence-like flow instabilities even at vanishingly low Re (the purely-elastic limit) [13], the best known linear instability mechanisms require curved streamlines [14, 15]. For parallel shear flows, the laminar state was long believed to be linearly stable [16, 17]. Indeed, earlier search of purely elastic turbulence in those flows focused on nonlinear instabilities [18, 19].

Recent discovery of a center-mode (CM) linear instability in viscoelastic pipe and channel flows [20, 21] has shaken this view. The instability is inertioelastic (finite Re is required) but, at least in channel flow, it continues smoothly to a purely-elastic ($Re = 0$) instability [22]. EIT is probably not directly triggered by that instability. First, the CM instability is only found for a limited parameter region and requires extremely high Weissenberg number Wi for dilute solutions. Its parameter

domain does not match where EIT is typically found. Second, EIT structures grow from the wall regions, for which a wall-mode (WM) instability would be more intuitive [23]. However, the instability connects subcritically to a saddle-node bifurcation with an upper-branch solution resembling the so-called arrowhead structure in EIT [24]. For highly elastic fluids at low Re , recent experiments observed similar flow patterns as the unstable eigenmode of the instability, which supports this subcritical connection [25]. In a competing theory, transition to EIT was linked with the so-called viscoelastic nonlinear TS wave [26], which, at least at high Re , continues to the Newtonian TS wave [27]. In both scenarios, transition to EIT is believed to be subcritical and requires sufficiently large disturbances to trigger nonlinear effects. Moreover, those studies only focused on 2D flows. Although a form of EIT does exist in 2D, key EIT dynamics important for MDR is only captured in 3D [11].

We use direct numerical simulation (DNS) to explore different transition scenarios in plane Poiseuille flow, including transition to both IDT and EIT. We report that EIT can be triggered directly from a WM linear instability in both 2D and 3D flows. With varying Re , Wi , and disturbance magnitude, different nonlinear transition scenarios are also observed.

DNS is performed with a fixed pressure gradient along the x direction. Two no-slip parallel walls confine the flow in the y direction. Periodic boundaries are applied to x and z directions. The half-channel height l and Newtonian laminar centerline velocity U_{CL} are used as the characteristic length and velocity, respectively, and l/U_{CL} and ρU_{CL}^2 are used to scale time t and pressure p (ρ is fluid density). DNS seeks the time-dependent solution of the Navier-Stokes equation coupled with the FENE-P constitutive equation [28]:

$$\frac{D\mathbf{v}}{Dt} = -\nabla p + \frac{\beta}{Re} \nabla^2 \mathbf{v} + \frac{2(1-\beta)}{ReWi} (\nabla \cdot \boldsymbol{\tau}_p), \quad (1)$$

$$\nabla \cdot \mathbf{v} = 0, \quad (2)$$

$$\frac{Wi}{2} \left(\frac{D\boldsymbol{\alpha}}{Dt} - \boldsymbol{\alpha} \cdot \nabla \mathbf{v} - (\boldsymbol{\alpha} \cdot \nabla \mathbf{v})^T \right) = -\frac{b}{b+5} \boldsymbol{\tau}_p, \quad (3)$$

$$\boldsymbol{\tau}_p = \frac{b+5}{b} \left(\frac{\boldsymbol{\alpha}}{1 - \frac{\text{tr}(\boldsymbol{\alpha})}{b}} - \left(\frac{b}{b+2} \right) \boldsymbol{\delta} \right), \quad (4)$$

where α and τ_p are the polymer conformation and stress tensors, respectively. Nondimensional parameters include: $Re \equiv \rho U_{CL} l / \eta$, $Wi \equiv 2\lambda U_{CL} / l$, $\beta \equiv \eta_s / \eta$, and $b \equiv \max(\text{tr}(\alpha))$ (where η and η_s are the fluid and solvent viscosity, respectively, and λ denotes the polymer relaxation time). Polymer concentration is proportional to $1 - \beta$, $\text{tr}(\alpha)$ is proportional to the square of polymer end-to-end distance, and b defines the finite extensibility of polymer chains. We fix $\beta = 0.97$ and $b = 5000$ in this study. A hybrid method combining a total variation diminishing (TVD) finite difference scheme for the $\mathbf{v} \cdot \nabla \alpha$ term with pseudospectral discretization of all other terms is adopted, in which artificial diffusion is not used [23, 29]. DNS at different Re is performed with a fixed domain size $L_x \times L_y \times L_z = 8.485 \times 2 \times 2.711$ ($L_x \times L_y = 8.485 \times 2$ for 2D). For 3D, the numerical mesh is $N_x \times N_y \times N_z = 256 \times 131 \times 142$ and time step is $\delta t = 0.005$ and, for 2D, $N_x \times N_y = 1280 \times 369$ and $\delta t = 0.001$. The numerical resolution and procedure were thoroughly validated in our earlier studies [11, 23].

An initial velocity disturbance

$$(v_x^\dagger, v_y^\dagger, v_z^\dagger)|_{t=0} = \left(-\frac{\partial \Psi}{\partial y} \cos \theta, \frac{\partial \Psi}{\partial z'}, -\frac{\partial \Psi}{\partial y} \cos \theta \right) \quad (5)$$

is superposed on the viscoelastic laminar base flow to trigger instabilities. (Hereinafter, \dagger indicates deviation from the base flow.) The disturbance stream function is

$$\Psi = K f(y) \left(\frac{x'}{l_x} \right) z' \exp \left[-\left(\frac{x'}{l_x} \right)^2 - \left(\frac{z'}{l_z} \right)^2 \right], \quad (6)$$

where $l_x = l_z = 2$ sets its geometric size, $\theta = 0$ sets its orientation, and

$$(x', z') = (x \cos \theta - z \sin \theta, x \sin \theta + z \cos \theta). \quad (7)$$

The Cartesian coordinates (x, y, z) are defined with the channel center as the origin. The function

$$f(y) = (1 + y)^2 \exp(\beta_f (1 + y)^2) - (1 - y)^2 \exp(\beta_f (1 - y)^2) \quad (8)$$

adjusts the wall-normal dependence of the disturbance. With $\beta_f = -10$ used in this study, $f(y)$ peaks at $y \approx \pm 0.7$. K adjusts the disturbance magnitude. At $K = 1$, the maximum velocity disturbance is $\mathcal{O}(10^{-2})$. The disturbance is similar to that commonly used in bypass transition studies [30, 31] with modifications made in eqs. (5) and (8). For 2D flow, z in eq. (7) is set to 0. We emphasize that our reported instability behaviors do not rely on this particular disturbance form. This was confirmed by testing another form of disturbance. In particular, at sufficiently small disturbance magnitudes, both forms lead to the same linear instability.

Figure 1(a) shows the growth trajectories of the mean-square wall-normal velocity disturbance $\langle (v_y^\dagger(t))^2 \rangle_V$ ($\langle \cdot \rangle_V$

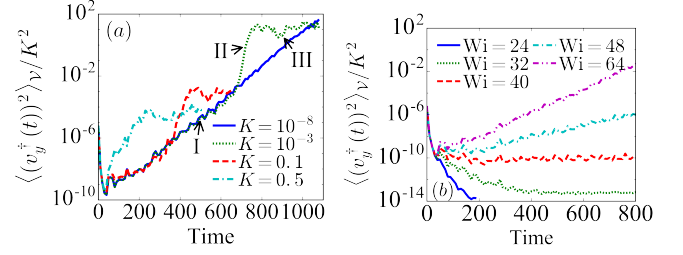


FIG. 1: Evolution of velocity disturbance from the perturbed laminar state in 2D at $Re = 3600$ with (a) varying K at $Wi = 64$ and (b) varying Wi at $K = 10^{-8}$.

denotes volume average) in high- Wi 2D flow with different initial disturbance magnitudes. The disturbance grows at all K values tested, down to $K = 10^{-8}$ at which the maximum velocity disturbance is ten orders of magnitude smaller than the base-flow velocity. Growth of infinitesimal disturbances is the defining feature of linear instability. At $K = 10^{-8}$, the disturbance grows exponentially with time (fig. 1(a) is semilogarithmic), which also confirms the existence of a linear inertioelastic instability (LIEI). We call it inertioelastic because both high Re and high Wi are required. (A small dip is seen at the short-time limit because the arbitrarily-chosen initial disturbance does not match the unstable eigenmode of the instability.) At $K = 10^{-3}$ and $K = 0.1$, the initial growth is still exponential. With $\langle (v_y^\dagger(t))^2 \rangle_V$ scaled by K^2 , growth trajectories over a wide range of K (10^{-8} to 10^{-1}) perfectly collapse in this exponential growth stage – i.e., $v_y^\dagger(t) \propto K$, which, once again, proves the linearity of the instability. Departure from exponential growth occurs later when the disturbance reaches the threshold for nonlinear effects. For the $K = 10^{-3}$ and $K = 0.1$ cases shown, the departure occurs at about the same $\langle (v_y^\dagger(t))^2 \rangle_V$ magnitude of $\sim \mathcal{O}(10^{-9})$. For a larger $K = 0.5$, the initial disturbance is large enough to trigger direct transition to the nonlinear inertioelastic instability (NIEI) without a noticeable exponential stage. After the nonlinear growth stage, all cases converge to a plateau corresponding to the EIT state previously found in 2D [11, 23, 32].

Figure 1(b) shows that, at $Re = 3600$, the linear instability only exists at $Wi > 40$, below which the disturbance decays. Interestingly, this critical Wi coincides with the minimal Wi for self-sustaining EIT to emerge in our earlier 3D DNS at the same parameters [11].

Typical flow structures for instability growth from the LIEI are shown in Figure 2. During the linear (exponential-growth) stage (I), thin inclined polymer sheets are closely attached to the wall, with the maximum $\text{tr}(\alpha)$ disturbance found at $y \approx \pm 0.8$. The sheets are sandwiched by two parallel trains of counter-rotating spanwise vortices. This is clearly a WM instability that differs from the CM instability from linear stability anal-

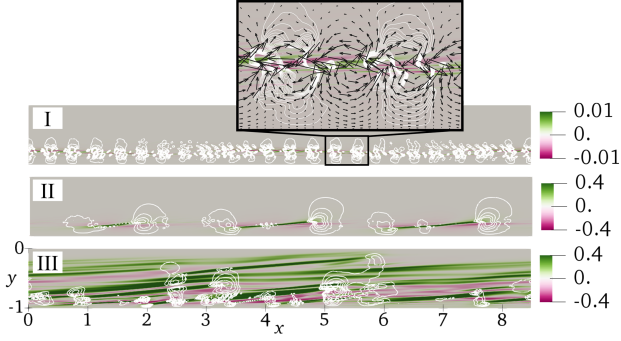


FIG. 2: Different stages of instability development (as marked in fig. 1 for $K = 10^{-3}$) in 2D flow (bottom half channel). Lines represent vortex strength Q contour levels [33, 34] (I: $2 \times 10^{-5} \sim 4 \times 10^{-4}$; II: $0.002 \sim 0.02$, III: $0.005 \sim 0.05$). Colors map to the $\text{tr}(\alpha)/b$ disturbance field. Arrows in the inset show x and y velocity disturbances.

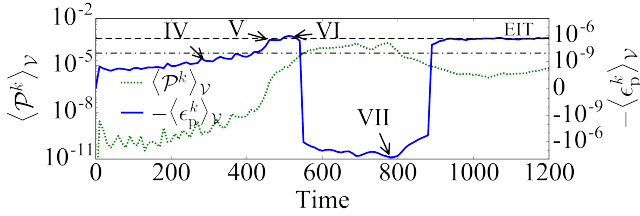


FIG. 3: Contributions to TKE growth from inertial ($\langle \mathcal{P}^k \rangle_V$) and elastic ($-\langle \epsilon_p^k \rangle_V$) mechanisms in 3D flow following the LIEI ($K = 0.05$, $\text{Re} = 3600$, and $\text{Wi} = 64$). Dot-dashed and dashed lines mark the $-\langle \epsilon_p^k \rangle_V$ magnitudes for the onset of NIEI and steady-state EIT, respectively.

ysis [20]. The structure is quasi-periodic with some level of chaos. Over the domain length L_x , one can count ≈ 23 periods, which translates to a wavenumber $k = 2\pi/L_x \times 23 \approx 17$. Previous studies mostly explored instabilities at $k \lesssim \mathcal{O}(1)$. The new LIEI occurs at a much smaller length scale than those previously searched. The small linear structures reorganize into $k = \mathcal{O}(1)$ structures with larger vortices and longer polymer sheets during nonlinear growth (II). Eventually, as $\langle (v_y^\dagger(t))^2 \rangle_V$ plateaus (III), the solution converges to the steady 2D EIT solution [23, 32], where the polymer sheets extend downstream and stack up in a lasagna configuration. This completes a pathway for EIT growth from a linear instability, which, to our knowledge, was never reported before.

The same LIEI, showing exponential growth of velocity disturbance in proportion to K , is also found in 3D flow down to the lowest $K = 10^{-8}$ tested. Figure 3 shows the inertial and elastic driving forces for turbulence growth from the LIEI using a turbulent kinetic energy (TKE) $\langle k \rangle_V \equiv (1/2)\langle \mathbf{v}' \cdot \mathbf{v}' \rangle_V$ (“ \prime ” indicates fluctuations w.r.t.

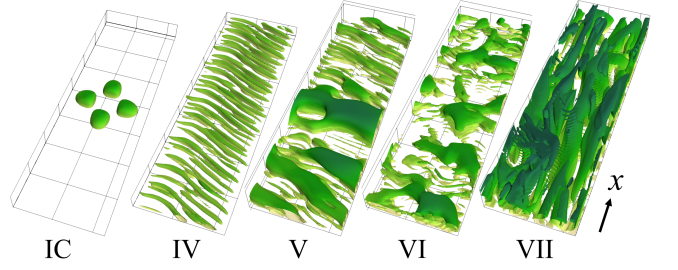


FIG. 4: Vortex evolution from the initial condition (IC) to different stages following the LIEI (as marked in fig. 3) in 3D flow (bottom half channel). Isosurfaces show vortex strength [33, 34] ($Q = 0.0005$ for IC and $Q = 0.005$ for the rest).

the ensemble average) balance [4, 11, 35]:

$$\frac{\partial \langle k \rangle_V}{\partial t} = \langle \mathcal{P}^k \rangle_V - \langle \epsilon_v^k \rangle_V - \langle \epsilon_p^k \rangle_V \quad (9)$$

where $\mathcal{P}^k \equiv -\langle v'_x v'_y \rangle (\partial \langle v_x \rangle / \partial y)$ is the TKE production by inertia, $\epsilon_v^k \equiv (2\beta/\text{Re})\langle \mathbf{\Gamma}' : \mathbf{\Gamma}' \rangle$ is its viscous dissipation, and $\epsilon_p^k \equiv (2(1-\beta)/(\text{ReWi}))\langle \boldsymbol{\tau}'_p : \mathbf{\Gamma}' \rangle$ is TKE conversion to elastic energy ($\mathbf{\Gamma} \equiv (1/2)(\nabla \mathbf{v} + (\nabla \mathbf{v})^T)$; $\langle \cdot \rangle$ denotes xz -average). Linear growth occurs at $t \lesssim 440$, which is mostly driven by elasticity as $-\langle \epsilon_p^k \rangle_V$ is positive and significantly higher than $\langle \mathcal{P}^k \rangle_V$. NIEI occurs at $t \approx 440$, where sudden jumps are found in both $-\langle \epsilon_p^k \rangle_V$ and $\langle \mathcal{P}^k \rangle_V$. With varying K (not shown), the onset time of the nonlinear departure changes, but it occurs at the same threshold magnitude of $-\langle \epsilon_p^k \rangle_V$ (dot-dashed line in fig. 3). At $t \approx 465$, $-\langle \epsilon_p^k \rangle_V$ reaches a plateau that matches 3D EIT found previously [11, 23]. At $t \approx 540$, $-\langle \epsilon_p^k \rangle_V$ quickly drops to negative – elasticity starts to suppress turbulence, leaving inertia as the only driving force for instability. This period of IDT is temporary and the flow eventually returns to EIT as its steady state. At sufficiently high K , the LIEI is bypassed to allow direct NIEI or, at larger K , direct transition to IDT. We will call the latter a nonlinear inertia-driven instability (NIDI), where a rapid rise in $\langle \mathcal{P}^k \rangle_V$ and negative $-\langle \epsilon_p^k \rangle_V$ follow the initial disturbance.

Figure 4 shows the evolving vortex configuration at different stages in fig. 3. During the linear growth stage (IV), the imposed, highly localized disturbance (IC) quickly transforms to narrow, finger-like vortices spreading across the near-wall layer. The structure closely resembles that of linear growth in 2D (fig. 2(I)), except for a small tilt in z . Our test with another disturbance form results in a different, but also weak, z -dependence. We thus conclude that the z -dependence is insignificant and the instability is still fundamentally 2D. The onset of NIEI is marked by the emergence of large spanwise rolls (V). The rolls initially reflect their 2D origin but quickly become z -dependent as EIT is reached (VI). Separation

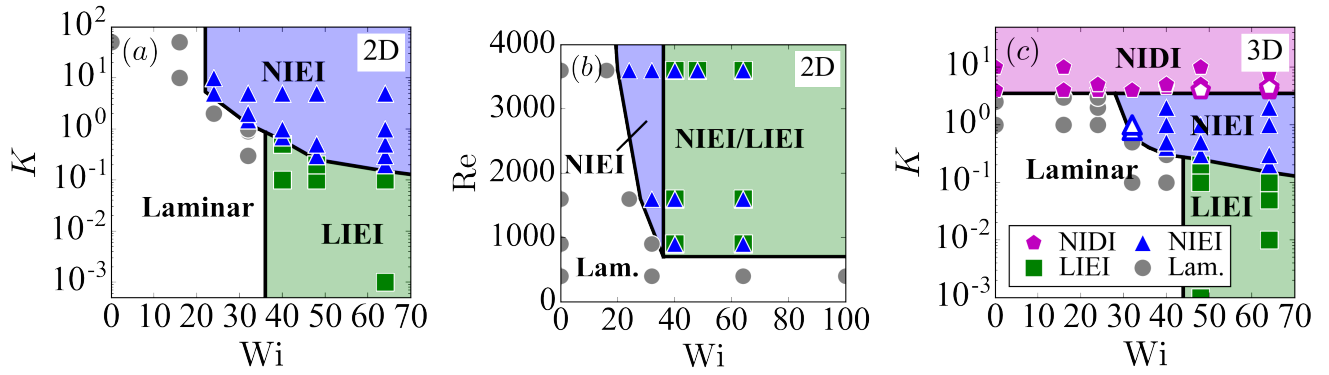


FIG. 5: Instability scenarios: (a) 2D flow in the K - Wi space ($Re = 3600$); (b) 2D flow in the Re - Wi space ($K = 10^{-8}$ for LIEI; $K = 5$ for NIEI); (c) 3D flow in the K - Wi space ($Re = 3600$). Empty symbols indicate that the resulting turbulent state lasts for < 400 time units.

from 2D dynamics is expected. Indeed, 3D features of EIT are critical for MDR behaviors [11]. During the transient IDT period (VII), spanwise rolls are replaced by streamwise vortices.

We now explore instability behaviors in broader Wi and Re ranges. For 2D flow at $Re = 3600$ (fig. 5(a)), the LIEI occurs at $Wi \gtrsim 40$. The critical Wi is independent of K , as expected for a linear instability. (Although not included in fig. 5, all LIEI cases are tested for $K = 10^{-8}$.) Larger disturbances trigger direct transition to the NIEI, which is found for Wi down to 24. Figure 5(b) shows that the critical Wi for the LIEI is also constant over varying Re . For comparison, the original experiments by Samanta *et al.* [9] reported that for the same polymer solution, transition to EIT occurs at the same shear rate (i.e., same Wi) and does not depend on the disturbance magnitude. The NIEI is found in the same region when a larger disturbance is used, but it also extends to lower Wi , which indicates a subcritical bifurcation. The minimal Wi for NIEI decreases with increasing Re . The lowest Re where we find instability, linear or nonlinear, is 900. The existence of a finite- Re threshold indicates the necessity of inertia in the instabilities, despite the seemingly more important role of elasticity. For this reason, the instabilities are considered inertioelastic.

For 3D flow, the Wi -dependence of LIEI and NIEI (fig. 5(c)) is similar to the 2D case, except that the critical Wi is slightly higher. This is likely due to the coarser resolution used in 3D DNS, which under-resolves the stress shock fronts [23]. Larger disturbances cause the NIDI. Its threshold K appears insensitive to increasing Wi , which supports the earlier finding that the laminar-IDT boundary is invariant with Wi [36, 37]. At high Wi , however, the resulting IDT only exists as short transients (replaced by EIT later). Shortening of IDT periods with increasing Wi reflects the turbulence-suppression role of elasticity in that regime, whereas for NIEI, the threshold K decreases with Wi – i.e., elasticity is a destabilizing force.

Coexisting inertial and inertioelastic transitions were also reported by Samanta *et al.* [9] in their low polymer concentration cases: transition to EIT occurs when no extra disturbance was introduced, but with larger disturbances the transition behavior matches that of IDT.

Our most important finding is that EIT can be triggered directly from a WM linear instability of the laminar state. In this statement, we restrict the term “EIT” to the dominant flow type of MDR and other high- Wi turbulent states in experimentally relevant parameter regimes for the DR problem, while recognizing the possibility that other linear instabilities, such as the CM instability [20, 21], could lead to other, so-far unknown, self-sustaining dynamics that are also inertioelastic in nature. The finding contradicts the prevalent notion that transition to turbulence in viscoelastic fluids, like in Newtonian fluids, must be subcritical. It also clearly portrays the relationship between different flow states and their relative stability, which paves the way for fully decoding the dynamics of high- Wi viscoelastic turbulence.

Acknowledgments – The authors acknowledge the financial support from the Natural Sciences and Engineering Research Council of Canada (NSERC; Nos. RGPIN-2014-04903 and RGPIN-2022-04720) and the allocation of computing resources awarded by the Digital Research Alliance of Canada (www.alliancecan.ca). The computation is made possible by the facilities of the Shared Hierarchical Academic Research Computing Network (SHARCNET: www.sharcnet.ca). Our viscoelastic DNS code is based on the Newtonian code **ChannelFlow 2.0** (<https://www.channelflow.ch>) developed by John Gibson, Tobias M. Schneider and co-workers.

* corresponding author, Email: xili@mcmaster.ca; <http://www.xiresearch.org>

[1] S. A. Orszag, Accurate solution of the Orr–Sommerfeld

- stability equation, *J. Fluid Mech.* **50**, 689–703 (1971).
- [2] M. Nishioka and M. Asai, Some observations of the subcritical transition in plane poiseuille flow, *J. Fluid Mech.* **150**, 441 (1985).
 - [3] P. S. Virk, Drag reduction fundamentals, *AIChE J.* **21**, 625 (1975).
 - [4] L. Xi, Turbulent drag reduction by polymer additives: Fundamentals and recent advances, *Phys. Fluids* **31**, 121302 (2019).
 - [5] W. Li, L. Xi, and M. D. Graham, Nonlinear travelling waves as a framework for understanding turbulent drag reduction, *J. Fluid Mech.* **565**, 353 (2006).
 - [6] K. Kim, R. J. Adrian, S. Balachandar, and R. Sureshkumar, Dynamics of hairpin vortices and polymer-induced turbulent drag reduction, *Phys. Rev. Lett.* **100**, 134504 (2008).
 - [7] L. Zhu, H. Schrobdsdorff, T. M. Schneider, and L. Xi, Distinct transition in flow statistics and vortex dynamics between low- and high-extent turbulent drag reduction in polymer fluids, *J. Non-Newton. Fluid Mech.* **262**, 115 (2018).
 - [8] L. Zhu and L. Xi, Vortex dynamics in low- and high-extent polymer drag reduction regimes revealed by vortex tracking and conformation analysis, *Phys. Fluids* **31**, 095103 (2019).
 - [9] D. Samanta, Y. Dubief, M. Holzner, C. Schäfer, A. N. Morozov, C. Wagner, and B. Hof, Elasto-inertial turbulence, *Proc. Natl. Acad. Sci. U. S. A.* **110**, 10557 (2013).
 - [10] G. H. Choueiri, J. M. Lopez, and B. Hof, Exceeding the asymptotic limit of polymer drag reduction, *Phys. Rev. Lett.* **120**, 124501 (2018).
 - [11] L. Zhu and L. Xi, Nonasymptotic elastoinertial turbulence for asymptotic drag reduction, *Phys. Rev. Fluids* **6**, 014601 (2021).
 - [12] B. Chandra, V. Shankar, and D. Das, Early transition, relaminarization and drag reduction in the flow of polymer solutions through microtubes, *J. Fluid Mech.* **885**, A47 (2020).
 - [13] A. Groisman and V. Steinberg, Elastic turbulence in a polymer solution flow, *Nature* **405**, 53 (2000).
 - [14] P. Pakdel and G. H. McKinley, Elastic instability and curved streamlines, *Phys. Rev. Lett.* **77**, 2459 (1996).
 - [15] L. Xi and M. D. Graham, A mechanism for oscillatory instability in viscoelastic cross-slot flow, *J. Fluid Mech.* **622**, 145 (2009).
 - [16] A. N. Morozov and W. van Saarloos, An introductory essay on subcritical instabilities and the transition to turbulence in visco-elastic parallel shear flows, *Phys. Rep.* **447**, 112 (2007).
 - [17] T. C. Ho and M. M. Denn, Stability of plane Poiseuille flow of a highly elastic liquid, *J. Non-Newton. Fluid Mech.* **3**, 179 (1977).
 - [18] L. Pan, A. Morozov, C. Wagner, and P. E. Arratia, Nonlinear elastic instability in channel flows at low Reynolds numbers, *Phys. Rev. Lett.* **110**, 174502 (2013).
 - [19] B. Qin, P. F. Salipante, S. D. Hudson, and P. E. Arratia, Flow resistance and structures in viscoelastic channel flows at low Re, *Phys. Rev. Lett.* **123**, 194501 (2019).
 - [20] P. Garg, I. Chaudhary, M. Khalid, V. Shankar, and G. Subramanian, Viscoelastic pipe flow is linearly unstable, *Phys. Rev. Lett.* **121**, 024502 (2018).
 - [21] M. Khalid, I. Chaudhary, P. Garg, V. Shankar, and G. Subramanian, The centre-mode instability of viscoelastic plane Poiseuille flow, *J. Fluid Mech.* **915**, A43 (2021).
 - [22] M. Khalid, V. Shankar, and G. Subramanian, Continuous Pathway between the Elasto-Inertial and Elastic Turbulent States in Viscoelastic Channel Flow, *Phys. Rev. Lett.* **127**, 134502 (2021).
 - [23] L. Zhu and L. Xi, Inertia-driven and elastoinertial viscoelastic turbulent channel flow simulated with a hybrid pseudo-spectral/finite-difference numerical scheme, *J. Non-Newton. Fluid Mech.* **286**, 104410 (2020).
 - [24] J. Page, Y. Dubief, and R. R. Kerswell, Exact Traveling Wave Solutions in Viscoelastic Channel Flow, *Phys. Rev. Lett.* **125**, 154501 (2020).
 - [25] G. H. Choueiri, J. M. Lopez, A. Varshney, S. Sankar, and B. Hof, Experimental observation of the origin and structure of elastoinertial turbulence, *Proceedings of the National Academy of Sciences of the United States of America* **118**, e2102350118 (2021).
 - [26] A. Shekar, R. M. McMullen, B. J. McKeon, and M. D. Graham, Self-sustained elastoinertial Tollmien-Schlichting waves, *J. Fluid Mech.* **897**, A3 (2020).
 - [27] A. Shekar, R. M. McMullen, B. J. McKeon, and M. D. Graham, Tollmien-Schlichting route to elastoinertial turbulence in channel flow, *Phys. Rev. Fluids* **6**, 093301 (2021).
 - [28] R. B. Bird, C. F. Curtis, R. C. Armstrong, and O. Hassager, *Dynamics of polymeric liquids*, 2nd ed., Vol. 2 (John Wiley & Sons, New York, 1987).
 - [29] L. Zhu, *Inertia- and elasticity-driven turbulence in viscoelastic fluids with high levels of drag reduction*, Ph.D. thesis, McMaster University (2019).
 - [30] A. Agarwal, L. Brandt, and T. A. Zaki, Linear and nonlinear evolution of a localized disturbance in polymeric channel flow, *J. Fluid Mech.* **760**, 278 (2014).
 - [31] D. Henningson, A. Lundbladh, and A. Johansson, A mechanism for bypass transition from localized disturbances in wall-bounded shear flows, *J. Fluid Mech.* **250**, 169 (1993).
 - [32] S. Sid, V. E. Terrapon, and Y. Dubief, Two-dimensional dynamics of elasto-inertial turbulence and its role in polymer drag reduction, *Phys. Rev. Fluids* **3**, 011301 (2018).
 - [33] J. C. R. Hunt, A. A. Wray, and P. Moin, Eddies, stream, and convergence zones in turbulent flows, in *Proceedings of the Summer Program* (Center for Turbulence Research, Stanford, CA, 1988) pp. 193–208.
 - [34] L. Zhu and L. Xi, Vortex axis tracking by iterative propagation (VATIP): a method for analyzing three-dimensional turbulent structures, *J. Fluid Mech.* **866**, 169 (2019).
 - [35] L. Zhu, X. Bai, E. Krushelnysky, and L. Xi, Transient dynamics of turbulence growth and bursting: effects of drag-reducing polymers, *J. Non-Newton. Fluid Mech.* **266**, 127 (2019).
 - [36] L. Xi and M. D. Graham, Dynamics on the laminar-turbulent boundary and the origin of the maximum drag reduction asymptote, *Phys. Rev. Lett.* **108**, 028301 (2012).
 - [37] L. Xi and X. Bai, Marginal turbulent state of viscoelastic fluids: A polymer drag reduction perspective, *Phys. Rev. E* **93**, 043118 (2016).